ACCSCIENCE PUBLISHING

Journal of Seismic Exploration

ARTICLE

Fully automatic differentiation with coupling deep neural networks for full-waveform inversion

Pengyuan Sun[1,2], Jun Zheng[3], Jingyi Zhao[3], Ying Yang[3], and Yufeng Wang[3]*

[1]BGPInc., China National Petroleum Corporation, Zhuozhou, Hebei, China

[2]National Engineering Research Center of Oil and Gas Exploration Computer Software, Zhuozhou, Hebei, China

[3]Hubei Subsurface Multi-Scale Imaging Key Laboratory, China University of Geosciences, Wuhan, Hubei, China

(This article belongs to the *Special Issue: Advanced Artificial Intelligence Theories and Methods for Seismic Exploration*)

Abstract

Seismic full-waveform inversion (FWI) is a powerful technique used in geophysical exploration to infer subsurface properties. However, FWI often suffers from challenges such as cycle skipping and sensitivity to uncertainties in seismic observations. This study aims to tackle these challenges by developing a novel fully automatic differentiation (AD) strategy for seismic FWI, coupling U-Net-based reparameterization inspired by the deep image prior concept into a reformulated wave equation simulation framework utilizing recurrent neural networks (RNNs). We demonstrate that the U-Net reparameterization serves as a form of implicit regularization for FWI, mitigating the ill-posed nature of the inversion problem and enhancing the stability of the optimization process. In addition, the RNN reformulation offers a flexible approach for backpropagating the FWI misfit, allowing the gradient with respect to the velocity parameters to be computed using the AD capabilities inherent in deep learning frameworks. Through extensive experiments on synthetic datasets, we showcase the regularization effect of our proposed method, leading to improved inversion results in terms of accuracy and robustness. This study offers a promising avenue for enhancing the reliability and accuracy of FWI through the lens of deep learning methodologies.

Keywords: Full-waveform inversion; U-Net; Deep image prior; RNN-based FWI

***Corresponding author:**
Yufeng Wang
(wangyufeng@cug.edu.cn)

Citation: Sun P, Zheng J, Zhao J, Yang Y, Wang Y. Fully automatic differentiation with coupling deep neural networks for full-waveform inversion. *J Seismic Explor*. 2025;34(6):16-28.
doi: 10.36922/JSE025410085

Received: October 11, 2025

Revised: October 27, 2025

Accepted: October 28, 2025

Published online: November 19, 2025

1. Introduction

Seismic full-waveform inversion (FWI) stands out as a crucial method in geophysical exploration, allowing for high-resolution reconstruction of subsurface properties.[1-3] FWI iteratively refines velocity models by minimizing the difference between synthetic and observed data, employing gradient descent algorithms with gradients computed through the adjoint-state method.[4,5] Despite its significance, traditional FWI methods face challenges such as cycle-skipping and ill-posedness, making it difficult to accurately represent complex subsurface velocity models when initial models are inaccurate and

observations are incomplete or contaminated with noise.[6-8] Moreover, computation of gradients in traditional FWI through the adjoint state method can be cumbersome, requiring formulation for each wave equation, making numerical implementation challenging and prone to errors.[9,10]

Deep learning has emerged as a promising approach in seismic FWI, offering novel solutions to longstanding challenges in conventional seismic inversion.[11,12] By leveraging annotated seismic data pairs consisting of observed seismogram and corresponding subsurface models, supervised learning-based FWI methods train neural networks to learn the complex mapping between seismic data and subsurface properties.[13,14] However, supervised learning FWI heavily relies on the availability of large volumes of labeled training data. Obtaining such datasets can be challenging and resource-intensive. Apart from directly mapping seismic data to inverted models, the integration of deep learning to aid seismic FWI has been intensively explored over the recent years. This includes employing deep learning techniques for tasks such as data augmentation, model initialization, optimization, misfit function design, and learned regularization.[15-20] Supervised learning FWI shows promise but comes with limitations, such as reliance on high-quality labeled data and potential overfitting to specific datasets. In addition, its generalization to diverse geological settings can be problematic, limiting its effectiveness in real-world applications.[21,22]

Recent research has shifted toward physics-based deep learning FWI, where the neural network architecture or loss function encodes underlying physical principles. This approach aims to enhance the interpretability and generalization capabilities of FWI models by explicitly incorporating prior knowledge of the physics governing seismic wave propagation.[22-24] Physics-based deep learning for FWI can be approached in various ways. First, the utilization of deep learning tools like automatic differentiation (AD) and optimization methods has streamlined the FWI process, making it more straightforward and robust.[9,10,23,25-27] These techniques reformulate the time-marching finite-difference discretized wave equation as a recurrent neural network (RNN), which is often referred to as RNN-based FWI. This approach allows for the automatic calculation of gradients and facilitates efficient model updates. Second, integrating the wave equation into neural networks, as demonstrated by physics-informed neural networks (PINNs), enhances the ability of neural networks to grasp the fundamental physics of wave propagation, thereby improving inversion accuracy.[22,28,29] This approach allows the model to leverage known physical principles, reducing the reliance on large datasets and improving generalization across different scenarios. As a result, PINNs-based FWI can offer more robust solutions in complex subsurface environments, addressing some of the limitations faced by traditional methods. Third, the recently developed neural operator learning methods aim to approximate implicit operators defined by partial differential equations (PDEs) between functional spaces.[30,31] These methods can serve as a rapid surrogate for the wave equation, enhancing the efficiency of seismic inversion by reducing the need for multiple wave equation simulations.[24,32] In addition, the concept of deep image prior suggests that the architecture of a neural network itself can act as a potent prior for inversion tasks.[33-35] In the realm of linear inversion, the deep neural network (DNN) parameterization method is referred to as regularization by architecture, where the spatial and temporal features of DNNs are harnessed to adjust inversion results to meet specific expectations.[34] The efficacy of regularization by architecture relies, to some extent, on the meticulous design of network architectures. In the geophysics community, the use of DNNs, particularly convolutional neural networks (CNNs), has gained traction for regularized estimation in FWI. This approach leverages the inherent structure of CNNs to capture spatial dependencies in geophysical data, improving the accuracy and robustness of subsurface model estimations.[36-41]

In this study, we propose a novel seismic FWI framework with coupling DNNs for reparameterization and reformulation, termed fully automatic differentiation-based FWI (FAD-FWI). In this approach, the subsurface velocity models are reparameterized by the weights of DNNs and then fed into an RNN-based FWI module. The seamless integration of these two neural networks enables FAD, allowing the weights of the DNNs to be updated by backpropagating the misfit between synthetic and observed seismograms. The integration of DNNs and RNNs enhances inversion outcomes by eliminating the need for manual tuning of regularization parameters and the reliance on error-prone adjoint state methods. In addition, the FAD-FWI framework offers flexibility in handling complex geological structures and can potentially outperform traditional FWI techniques by exploiting the strengths of deep learning for regularization and optimization. By harnessing the hierarchical feature extraction capabilities of the U-Net, our proposed FAD-FWI method can effectively map a Gaussian random field (GRF) input to the inverted velocity model, aligning it with seismic observations through RNN-based FWI. FAD-FWI outperforms traditional FWI with lower dependency on initial model estimations and better robustness in the face of uncertainties in seismic observations. Through extensive

experiments on synthetic seismic datasets, we demonstrate that FAD-FWI provides more accurate subsurface models and offers greater computational flexibility compared to conventional FWI methods. The main contributions of this work are twofold. We propose the FAD-FWI architecture, which overcomes a key limitation of prior deep learning-based FWI methods. By employing a linear activation in the final layer, our model directly outputs velocity values in a physically realistic range, eliminating the need for a problem-dependent scaling factor. In addition, we develop a fully AD framework that seamlessly integrates a DNN-based model parameterization with the physics of wave propagation. This unified approach automatically computes the gradients of the FWI objective function through both the U-Net and the wave equation solver, removing the dependency on manually derived and implemented adjoint-state equations.

2. Methodology

2.1. FWI with regularization

Seismic FWI seeks to estimate subsurface properties by iteratively updating the velocity model until synthetic seismic data closely match the observed seismic data. FWI minimizes an objective function that measures the discrepancy between recorded and simulated seismic data. This function typically combines a data-misfit term with regularization to ensure stability and to guide the solution. Mathematically, the objective function can be expressed as:

$$\mathcal{J}(m)=\frac{1}{2}\sum_{s,r} d_{obs}(x_r,t;x_s)-d_{cal}(x_r,t;x_s;m)^2+\lambda\mathcal{R}(m) \quad \text{(I)}$$

Where d_{obs} and d_{cal} are observed wavefield and the calculated wavefield recorded at receivers associated with sources , respectively. R denotes the regularization term on velocity model m with weighting coefficient λ. The handcrafted regularization terms, often based on expert knowledge or empirical observations, help guide the inversion process toward solutions that are physically plausible and consistent with prior expectations. However, these priors can sometimes be overly general, as the models generated using their associated probability density functions may encompass a broader range of possibilities than those specifically relevant to geophysics. As a result, there is a risk of introducing biases or inaccuracies into the inversion results, particularly when the priors do not accurately capture the true distribution of subsurface properties in the study area.[42,43] This limitation has prompted researchers to explore alternative approaches to regularization that can adaptively incorporate domain-specific knowledge and better capture the complexities of subsurface structures in geophysical inversion tasks.

2.2. FWI with U-Net reparameterization

As demonstrated in the seminal work of deep image prior, a randomly-initialized neural network can serve as effective prior in inverse problems.[33,34] In this study, we employ U-Net reparameterization for seismic FWI with the following objective function:

$$\mathcal{J}(\theta)=\frac{1}{2}\sum_{s,r} d_{obs}(x_r,t;x_s)-d_{cal}\left(x_r,t;x_s;\mathcal{N}(z;\theta)\right)^2 \quad \text{(II)}$$

Where velocity model is reparameterized by a U-Net $N(z;\theta)$ with weights θ and fixed latent variable z. In this study, we use a latent variable z generated by GRF. In contrast to traditional FWI with the velocity m updated in model space, the proposed FAD-FWI updates the U-Net weights θ iteratively to match the observed data d_{obs} using a gradient-based optimization method with the gradient computed through the chain rule as follows:

$$\frac{\partial\mathcal{J}}{\partial\theta}=\left(\frac{\partial m}{\partial\theta}\right)^T\frac{\partial\mathcal{J}}{\partial m}=\left(\frac{\partial m}{\partial\theta}\right)^T\sum_{t=1}^{N_t}\frac{\partial\mathcal{J}}{\partial u_t}\frac{\partial A(m)}{\partial m}u_{t-1} \quad \text{(III)}$$

Here, we assume the time-marching finite-difference discretization of the wave equation $u_t = A(m)\ u_{t-1} + s_{t-1}$ with $A(m)$ being the finite difference coefficient matrix. In general, regularization by U-Net architecture ensures that the inverted subsurface models maintain consistency with observed seismic data while also achieving desired properties such as spatial coherence and smoothness.[36,38,41] The input to the U-Net-reparameterized FWI consists of GRF realizations of random latent variables, with dimensions matching those of the velocity model. In this study, GRF has a covariance kernel function as follows:

$$C_\alpha(d)=\sigma^2\frac{2^{1-\alpha}}{\Gamma(\alpha)}\left(\sqrt{2\alpha}\frac{d}{\beta}\right)^\alpha K_\alpha\left(\sqrt{2\alpha}\frac{d}{\beta}\right) \quad \text{(IV)}$$

Where σ is the variance of the Gaussian process, α is known as the smoothness of GRF.[44,45] The constants used in the GRF kernel are determined by the complexity of the velocity model. Figure 1 presents the GRF latent variables with different smoothness, (a) α = 1.0, (b) α = 3.0, and (c) α = 5.0, respectively. In this study, we let α = 3.0 for all experiments. The U-Net architecture consists of an encoder-decoder structure: the encoder extracts features through a series of convolutional and downsampling layers, while the decoder upsamples the features to recover spatial resolution. Skip connections between corresponding layers in the encoder and decoder allow for detailed feature preservation.[46,47] The output of the U-Net is the predicted velocity model, which is subsequently fed into the FWI module to ensure that the synthetic data

match the observed data. In this U-Net reparameterization scheme, the U-Net serves as a regularizer, leveraging its inductive biases, such as spatial consistency and hierarchical feature extraction. These biases help preserve important structural patterns in the velocity model, promoting smoother and more geologically plausible solutions. By incorporating this learned regularization, the FWI process becomes more stable and less prone to overfitting, improving the accuracy and robustness of the inversion results.

2.3. FAD-based FWI

U-Net-reparameterized FWI leverages the inductive biases of the U-Net architecture, enhancing the accuracy and robustness of the inversion process. However, challenges arise when coupling the gradients of DNNs $\partial m/\partial \theta$ with that of the PDEs $\partial J/\partial m$, where the former is typically computed using backpropagation by AD within deep learning framework,[48] whereas the latter is commonly derived through the adjoint-state method.[4] Fortunately, the recently developed RNN-based FWI reformulates FWI into an RNN, enabling the gradient calculation of velocity parameters using AD as well.[23,25] The schematic architecture of the proposed FAD-FWI is shown in Figure 2, which seamlessly integrates two parts, with a U-Net architecture playing a pivotal role in reparameterizing the velocity model and an RNN enabling the gradients with respect to inversion parameters calculated by AD in a modern deep learning framework. This integrated approach holds promise for overcoming traditional FWI limitations and advancing the capabilities of seismic imaging in characterizing subsurface properties. In our proposed framework, two neural networks are combined, allowing the gradient of the cost function with respect to the U-Net weights to be fully computed through AD. This seamless gradient calculation eliminates the need for manual derivation of adjoint equations, enabling efficient updates to the U-Net weights during the inversion process. This is why we refer to the method as FAD-FWI, as it takes advantage of AD to optimize both the velocity model and neural network parameters simultaneously, streamlining the FWI workflow.

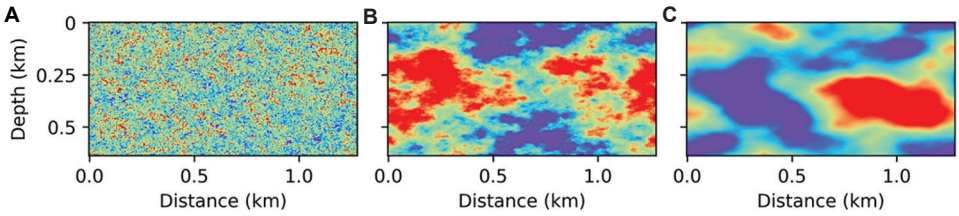

Figure 1. The Gaussian random field latent variables with different smoothness: (A) α = 1.0, (B) α = 3.0, and (C) α = 5.0, respectively

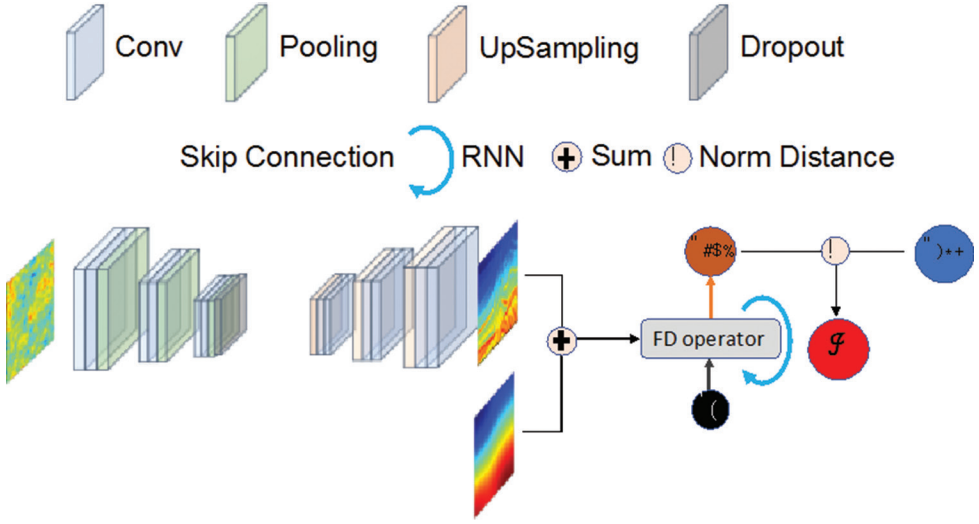

Figure 2. The schematic architecture of the proposed FAD-FWI. The GRF latent variable is fed into an encoder to generate a fused feature map, which is decoded and subsequently directed into an RNN-FWI module. The gradient of the cost function with respect to the U-Net weights is fully computed through AD. The plot of the RNN-based FWI module is adopted from Ref.[25]

Abbreviations: AD: Automatic differentiation; FAD: Fully automatic differentiation; FWI: Full-waveform inversion; GRF: Gaussian random field; RNN: Recurrent neural network.

3. Numerical examples

3.1. FAD-FWI regularized by U-Net architecture

In the first experiment, we aim to demonstrate the advantages of our proposed FAD-FWI framework regularized by the U-Net architecture compared to generative neural networks (GNNs). Specifically, we seek to verify that the inductive biases of U-Net, such as its ability to capture spatial hierarchies and maintain structural consistency, provide more robust regularization, and lead to more accurate velocity model predictions. By comparing the performance of FAD-FWI with U-Net regularization against GNN, we will highlight its effectiveness in producing geologically plausible models while improving the stability and convergence of the inversion process. The optimization configuration is consistent across all experiments. We use the Adam optimizer to minimize the objective function. The learning rate is set to 0.01 and kept constant throughout the inversion process. Each experiment is run for a fixed budget of 2000 iterations, which is empirically determined to be sufficient for the loss to converge in all tested scenarios.

We utilize an angular unconformity geological model shown in Figure 3A to demonstrate the superiority of our proposed FAD-FWI framework, regularized by the U-Net architecture (FAD-FWI-U-Net), in comparison to the version regularized by a GNN (FAD-FWI-GNN) with varying scaling factors as developed by Zhu *et al.*[38] The scaling factors are critical for mapping the bounded output of the neural network to the physically meaningful range of velocity models. As pointed by Zhu *et al.*,[38] applying scaling factors to the output of neural networks depends on the physical parameters and units. The final layer of the neural network used a Tanh activation function, which constrains its output to the range [-1, 1]. To map this bounded output to a meaningful velocity perturbation, a scaling factor is required. In contrast, our primary proposed method, FAD-FWI-U-Net, uses a linear activation (*i.e.*, no activation function) in its final layer. This is a significant advantage, as it allows the network to output velocity values in an unbounded range directly, without the need to assume or tune a predefined scaling factor. This makes FAD-FWI-U-Net more robust and easier to apply to new datasets where the appropriate velocity range may not be known *a priori*.

Figure 3A and B present the velocity model and a homogeneous initial model for FWI, respectively. The seismic acquisition configuration includes a total of 20 shots indicated by red stars and 256 receivers indicated by white dots, as shown in Figure 3B. The inverted velocity model obtained by FAD-FWI-U-Net is displayed in Figure 3C, showcasing good agreement with the true model in Figure 3A. Figure 3D-F depicts the recovered

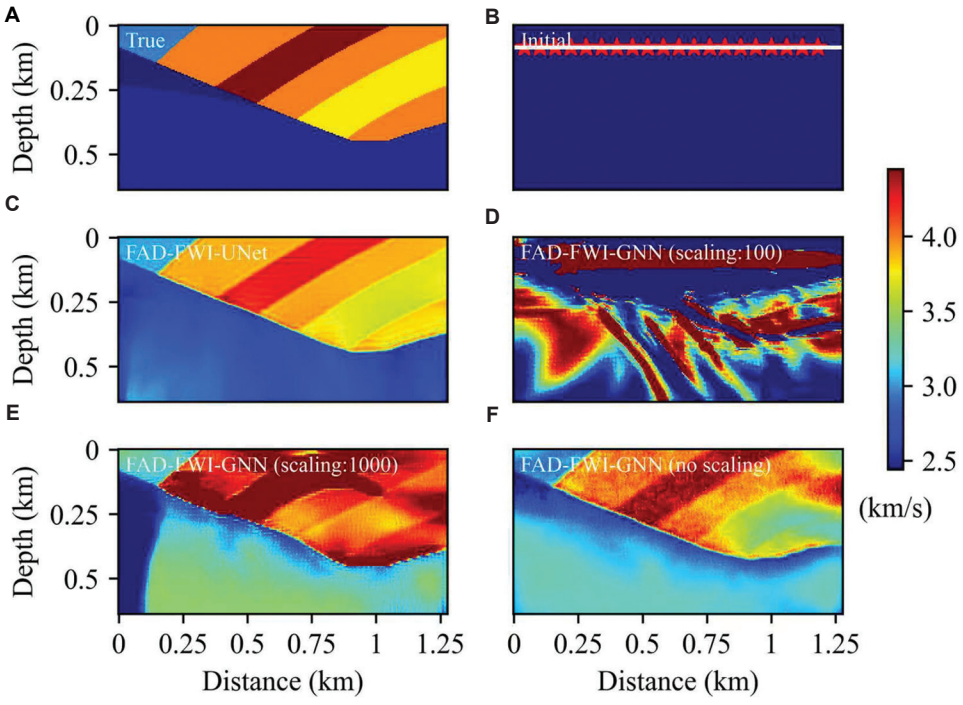

Figure 3. Comparison of inverted velocity models obtained using the proposed FAD-FWI-U-Net and FAD-FWI-GNN with different scaling factors. (A) The angular unconformity geological model; (B) homogeneous initial model; (C) inverted model by FAD-FWI-U-Net, and the inverted models by FAD-FWI-GNN with scaling factor of 100 (D), 1000 (E), and no scaling (F).
Abbreviations: FAD: Fully automatic differentiation; FWI: Full-waveform inversion; GNN: Generative neural network.

velocity models obtained by FAD-FWI-GNN with scaling factors of 100, 1000, and no scaling, respectively. Our results illustrate that FAD-FWI-U-Net can accurately reconstruct the velocity model without the need for predefined scaling, whereas FAD-FWI-GNN requires appropriate scaling for successful inversion; otherwise, it fails to accurately recover the velocity model. In addition, even after removing the Tanh activation in FAD-FWI-GNN, the inversion result shown in Figure 3F remains inferior to that of our proposed FAD-FWI-U-Net shown in Figure 3C. This difference is primarily due to the U-Net architecture, which effectively captures spatial hierarchies, preserves structural consistency, and offers more robust regularization for FWI. Figure 4 shows the loss curves for the proposed FAD-FWI-U-Net and FAD-FWI-GNN with scaling factors of 100, 1000, and no scaling. The results indicate that our proposed FAD-FWI-U-Net achieves a faster convergence rate after 500 iterations and a lower L1 error compared to FAD-FWI-GNN across different scaling factors. The impact of DNN architecture on parameterized FWI is a promising area for exploration in future work.

3.2. FAD-FWI across initial models

The second experiment focuses on evaluating the sensitivity of the proposed FAD-FWI method to the initial model estimation. Traditional FWI methods are often highly dependent on an accurate initial model; they tend to perform poorly when initialized with a less accurate model. In contrast, our FAD-FWI method, utilizing U-Net for parameterization, provides a strong regularizer that helps mitigate this dependency, enhancing inversion results even with suboptimal initial models. This robustness highlights the potential of our framework to improve inversion accuracy in challenging scenarios where initial model quality is compromised. In this experiment, we compare our proposed FAD-FWI method with traditional FWI implemented using Deepwave (https://ausargeo.com/deepwave/) and referred to as DW-FWI for simplicity.

Figure 5 presents the Marmousi velocity model, along with three different initial velocity models: smoothed model, smoothed 1D model, and homogeneous model, respectively. The acquisition configuration consists of 20 shots and 256 receivers, positioned at a depth of 85 m. Figure 6 presents the inverted velocity models obtained by DW-FWI and the proposed FAD-FWI with three different initial velocity models as shown in Figure 5. As the accuracy of the initial models decreases, the inversion results from DW-FWI deteriorate significantly. In contrast, our FAD-FWI approach achieves acceptable inversion results even when starting from a homogeneous initial model. Figure 7 depicts the comparison of the extracted

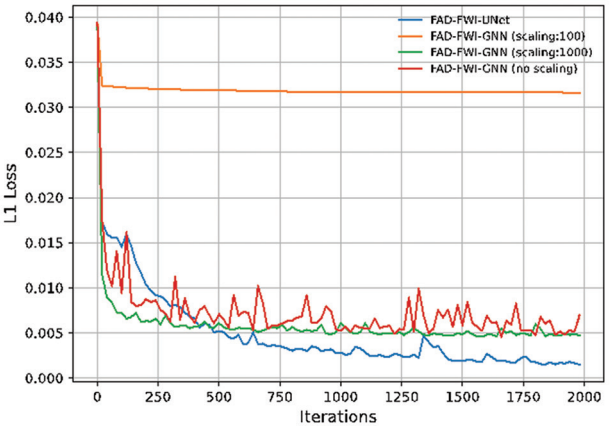

Figure 4. Comparison of the loss curves of the proposed FAD-FWI-U-Net and FAD-FWI-GNN with scaling factors of 100, 1000, and no scaling. We observe that FAD-FWI-GNN with a scaling factor of 100 fails to converge to lower L_1 errors due to improper scaling.
Abbreviations: FAD: Fully automatic differentiation; FWI: Full-waveform inversion; GNN: Generative neural network.

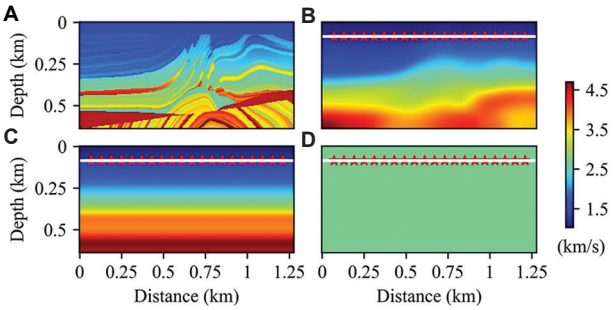

Figure 5. The Marmousi velocity model (A), along with three different initial velocity models: (B) smoothed model, (C) smoothed 1D model, and (D) homogeneous model. The acquisition configuration consists of 20 shots marked by red stars and 256 receivers by white dots, positioned at a depth of 85 m.

traces from Figure 6 at 0.25 km, 0.5 km, 0.75 km, and 1.0 km. It indicates that DW-FWI struggles to recover the velocity model when provided with an inaccurate homogeneous initial model, while the proposed FAD-FWI method still achieves satisfactory results, although with a slightly degraded quality. Figure 8 depicts the loss curves of DW-FWI and the proposed FAD-FWI with different initial velocity models. It is evident that conventional FWI without regularization exhibits a faster convergent rate at the early stages. However, the proposed FAD-FWI, which incorporates regularization by U-Net architecture, demonstrates lower L_1 errors overall. We further conduct sensitivity analysis of DW-FWI and the proposed FAD-FWI given a smoothed 1D initial model with different velocity perturbations from −30% to +30%. The inverted velocity models are displayed in Figure 9. The implication is

that DW-FWI is more susceptible to velocity perturbations compared to FAD-FWI. This experiment demonstrates the robustness of the proposed FAD-FWI to variations in the initial model estimation.

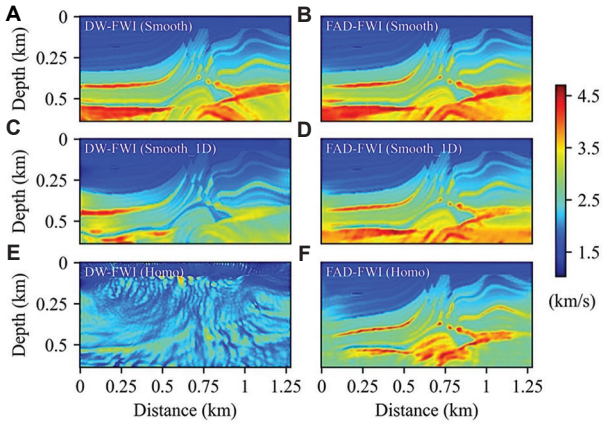

Figure 6. Comparison of inverted velocity models obtained using DW-FWI (A, C, E) and the proposed FAD-FWI (B, D, F) with different initial velocity models shown in Figure 5. From top to bottom, the rows correspond to inverted models with the smoothed model, smoothed 1D model, and the homogeneous model.
Abbreviations: DW: Deepwave; FAD: Fully automatic differentiation; FWI: Full-waveform inversion.

3.3. FAD-FWI across uncertainties in seismic observations

In our third experiment, we apply FAD-FWI to the 2D Overthrust velocity model, as depicted in Figure 10, in the presence of uncertainties in seismic observations such as noise and incomplete frequency components. We use a smoothed 1D initial model shown in Figure 10B for all tests. The acquisition configuration for this experiment is the same as in the previous experiments, with 20 shots and 256 receivers positioned at a depth of 85 m. Figure 11 presents shot gathers under various uncertainties in seismic observations, including clean and noisy data, as well as complete and incomplete data with missing frequencies below 2.5 Hz. The extracted traces at the left-most position, along with their spectra, are displayed alongside the shot gathers.

In this experiment, we perform FWI under conditions of uncertainty in seismic observations, including noise and incomplete frequency components. Figure 12 compares the inverted velocity models obtained by DW-FWI using different seismic observations with clean and noisy data, as well as complete and incomplete data with missing frequencies below 2.5 Hz. In this scenario, DW-FWI demonstrates acceptable performance with clean

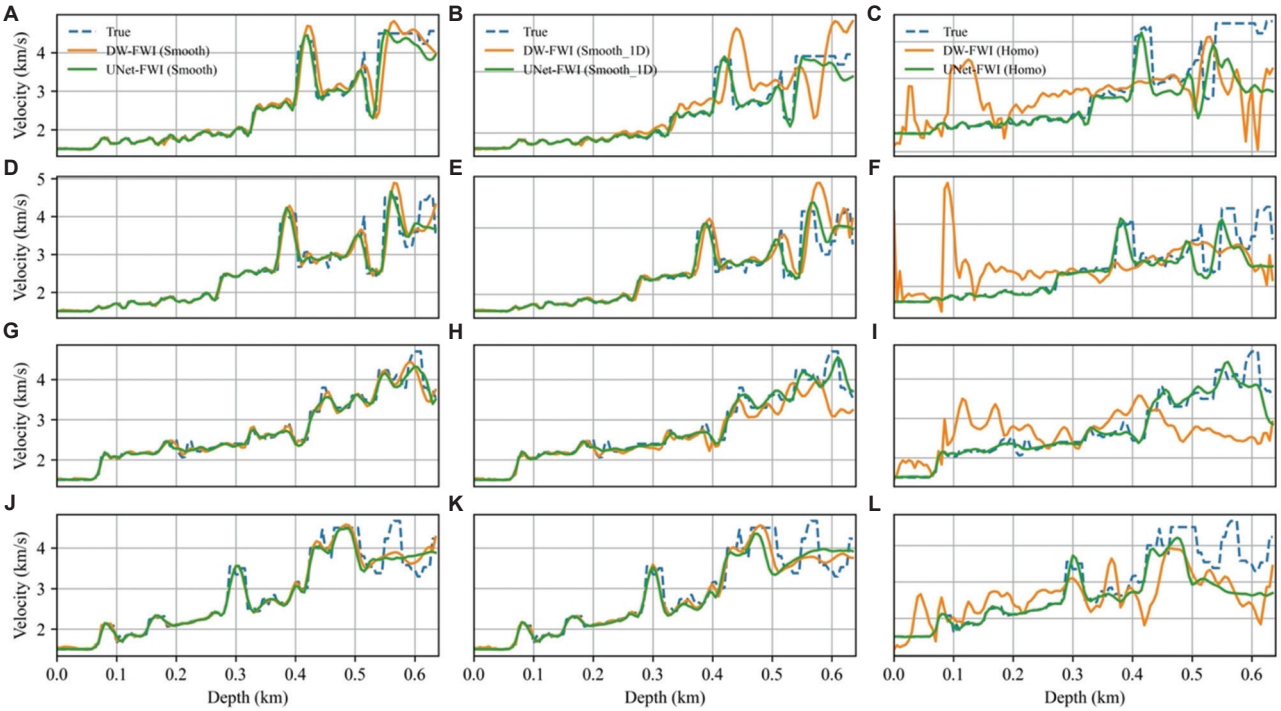

Figure 7. Comparison of the traces extracted from the inverted velocity models shown in Figure 6 at four trace locations. From top to bottom, the rows correspond to trace positions at 0.25 km (A, B, C), 0.5 km (D, E, F), 0.75 km (G, H, I), and 1.0 km (J, K, L). From left to right, the columns correspond to smoothed model (A, D, G, J), smoothed 1D model (B, E, H, K), and homogeneous model (C, F, I, L).
Abbreviations: DW: Deepwave; FAD: Fully automatic differentiation; FWI: Full-waveform inversion.

observations; however, its accuracy declines significantly when the seismic data are contaminated with random noise. It fails to recover the velocity model effectively when faced with both noisy data and missing low-frequency components. Figure 13 compares the inverted velocity models obtained using the proposed FAD-FWI with different seismic observations. The FAD-FWI method demonstrates robust performance, maintaining high-quality inversion results even as data quality degrades due to noise or incomplete frequency information. This resilience highlights the effectiveness of FAD-FWI in handling challenging data conditions. We provide quantitative evaluation metrics in Table 1 to assess the performance of the proposed FAD-FWI. The quantitative metrics mean squared error (MSE), structural similarity index measure (SSIM), and peak signal-to-noise ratio (PSNR) are defined by:

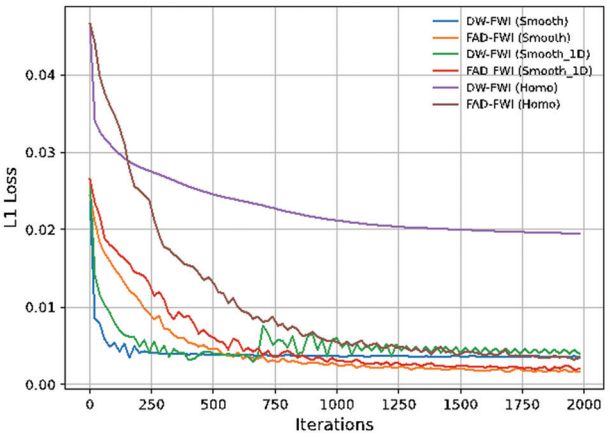

Figure 8. Comparison of the loss curves of DW-FWI and the proposed FAD-FWI with different initial velocity models.
Abbreviations: DW: Deepwave; FAD: Fully automatic differentiation; FWI: Full-waveform inversion.

$$MSE\left(m_{true},m_{inv}\right)=\frac{1}{N}\sum_{i=1}^{N}\left[m_{true}\left(i\right)-m_{inv}\left(i\right)\right]^{2} \quad \text{(V)}$$

$$PSNR\left(m_{true},m_{inv}\right)=10log_{10}\left(\frac{\left[MAX\left(m_{true}\right)-MIN(m_{true})\right]^{2}}{MSE\left(m_{true},m_{inv}\right)}\right) \quad \text{(VI)}$$

$$SSIM\left(x,y\right)=\frac{\left(2\mu_{x}\mu_{y}+C_{1}\right)\left(2\sigma_{xy}+C_{2}\right)}{\left(\mu_{x}^{2}+\mu_{y}^{2}+C_{1}\right)\left(\sigma_{x}^{2}+\sigma_{y}^{2}+C_{2}\right)} \quad \text{(VII)}$$

Where μ_x and μ_y are the mean intensities, and σ_x^2 and σ_y^2 are the variances of true model and the inverted model,

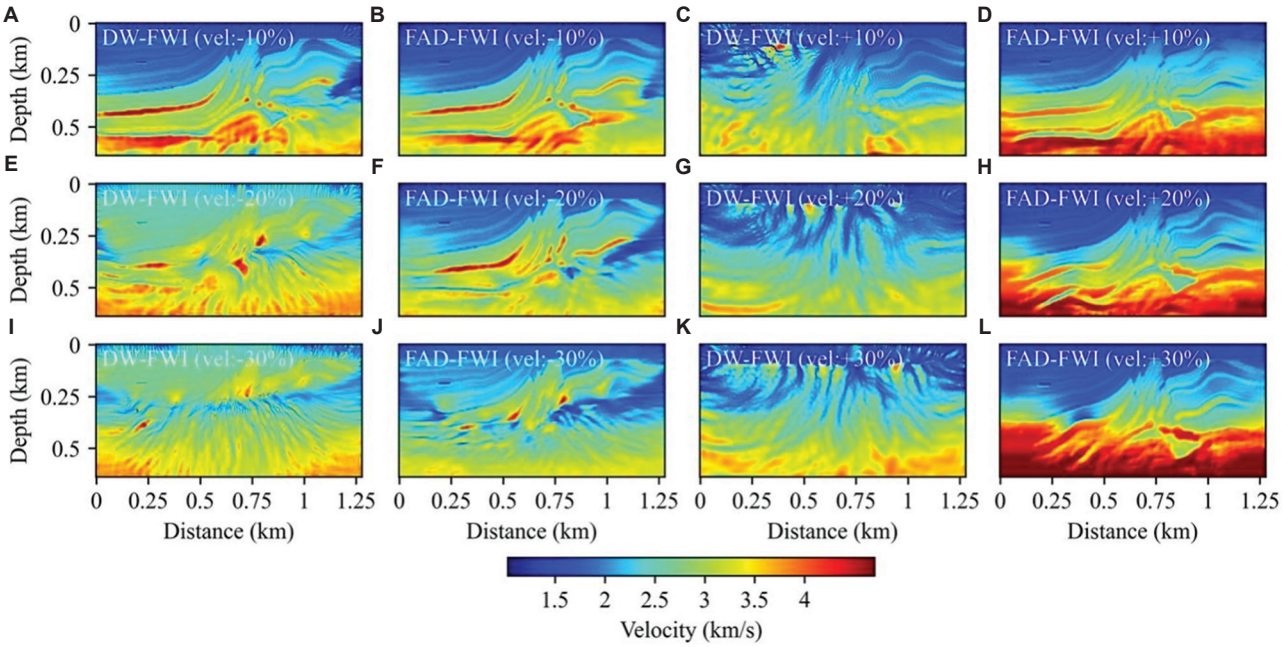

Figure 9. Sensitivity analysis of DW-FWI and the proposed FAD-FWI given smoothed 1D initial model with different velocity perturbations. The first column denotes the inverted models from DW-FWI with −10% (A), −20% (E), and −30% (I) deviated from the smoothed 1D initial model shown in Figure 5C. The second column denotes the inverted models from FAD-FWI with velocity perturbations of −10% (B), −20% (F), and −30%(J). The third and fourth columns correspond to the inverted models from DW-FWI and FAD-FWI with velocity perturbations of +10% (C and D), +20% (G and H), and +30% (K and L), respectively.
Abbreviations: DW: Deepwave; FAD: Fully automatic differentiation; FWI: Full-waveform inversion.

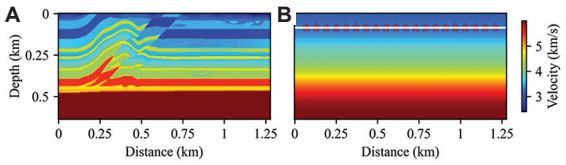

Figure 10. The Overthrust velocity model (A) and the smoothed 1D initial model (B). The acquisition configuration consists of 20 shots marked by red stars and 256 receivers by white dots, positioned at a depth of 85 m.

respectively. C_1 and C_2 are small constants stabilizing the division. The overall SSIM index is the mean of the SSIM values across all windows. The SSIM value ranges from −1 to 1, and a value of 1 indicates perfect structural similarity. This quantitative comparison suggests that the proposed FAD-FWI is more robust than DW-FWI in scenarios where observations lack low-frequency components and are contaminated by noise. In addition, we compare the

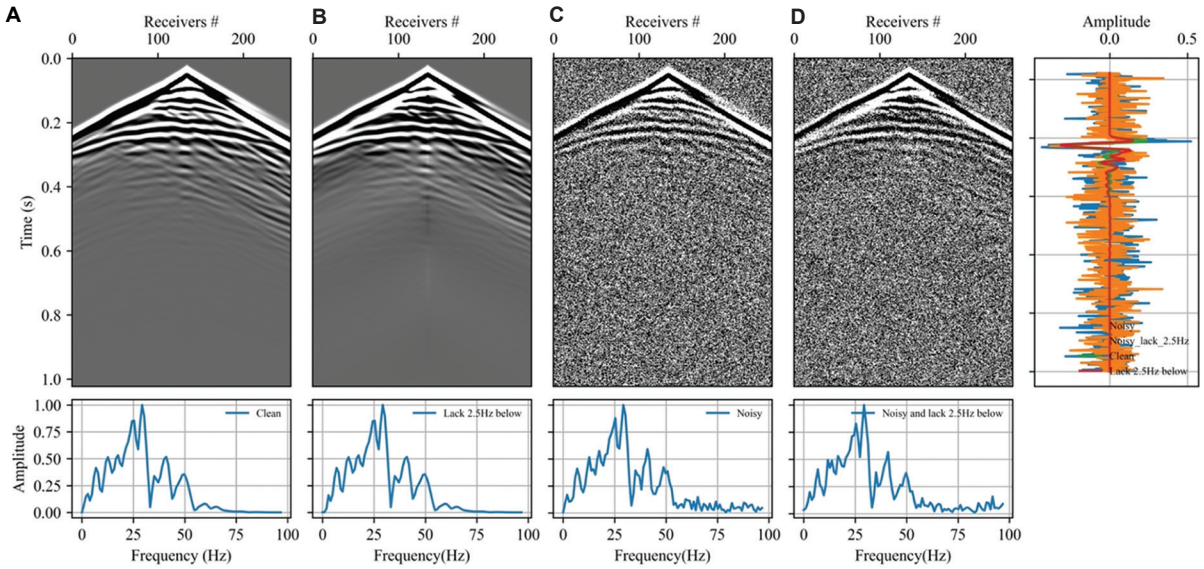

Figure 11. Shot gathers under various uncertainties in seismic observations, including clean data (A), clean data with missing frequencies below 2.5 Hz (B), noisy data with random noises $\sigma = 0.5\sigma_0$ (C), and noisy data with missing frequencies below 2.5 Hz (D). The extracted traces at the left-most position, along with their spectra, are displayed alongside the shot gathers.

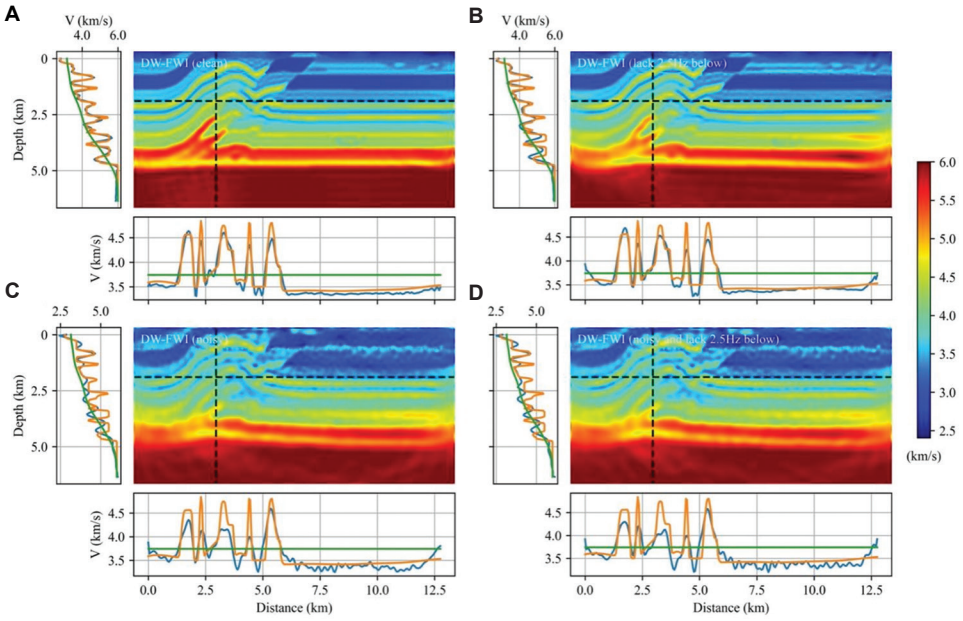

Figure 12. Comparison of inverted velocity models obtained using DW-FWI given different observations with clean data (A), clean data with missing frequencies below 2.5 Hz (B), noisy data with random noises $\sigma = 0.5\sigma 0$ (C), and noisy data with missing frequencies below 2.5 Hz (D).
Abbreviations: DW: Deepwave; FWI: Full-waveform inversion.

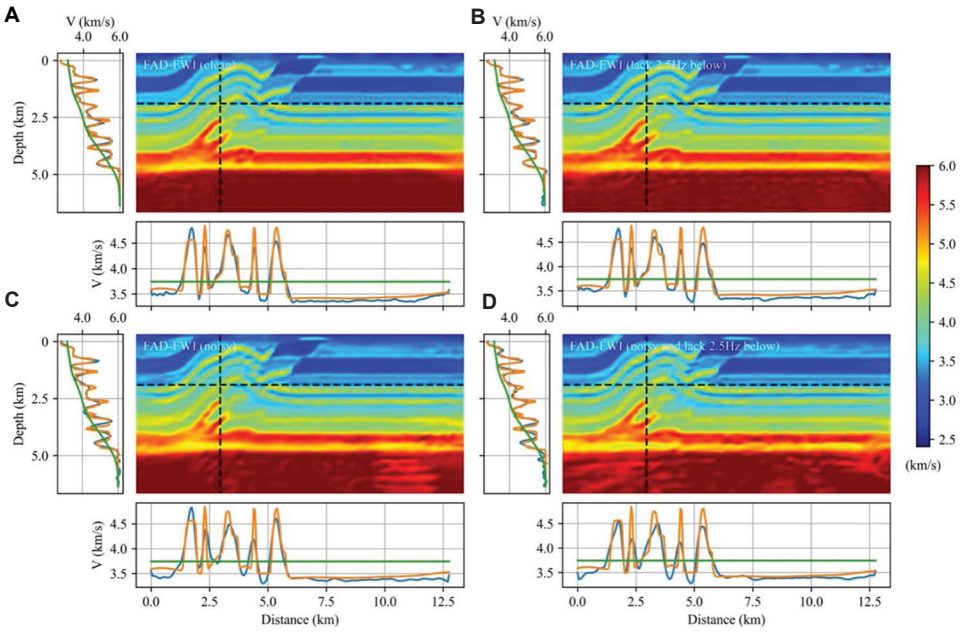

Figure 13. Comparison of inverted velocity models obtained using FAD-FWI given different observations with clean data (A), clean data with missing frequencies below 2.5 Hz (B), noisy data with random noises $\sigma = 0.5\sigma 0$ (C), and noisy data with missing frequencies below 2.5 Hz (D).
Abbreviations: FAD: Fully automatic differentiation; FWI: Full-waveform inversion.

Table 1. Quantitative evaluation metrics of the inverted velocity models obtained using DW-FWI and the proposed FAD-FWI under varying uncertainties in seismic observations

Methods	Metrics	MSE	SSIM	PSNR
DW-FWI	Full data	113.94	0.99	50.55
	Filtered data	200.87	0.98	48.09
	Noisy data	317.46	0.96	46.10
	Filtered noisy data	318.96	0.96	46.08
FAD-FWI	Full data	124.59	0.99	50.16
	Filtered data	132.03	0.99	49.91
	Noisy data	186.22	0.98	48.41
	Filtered noisy data	180.29	0.98	48.55

Abbreviations: DW: Deepwave; FAD: Fully automatic differentiation; FWI: Full-waveform inversion; MSE: Mean squared error; PSNR: Peak signal-to-noise ratio; SSIM: Structural similarity index measure.

runtime and memory usage for both DW-FWI and FAD-FWI. On an NVIDIA GeForce RTX 3080Ti (12 GB) GPU, the traditional DW-FWI method completed in 8 min and 31 s with a peak memory usage of 5.3 GB. In comparison, our proposed FAD-FWI method required 9 min and 6 s and 6.4 GB of memory. This represents a modest increase in runtime and memory usage for FAD-FWI, which is a reasonable trade-off given its significant improvements in accuracy and stability, as demonstrated by the quantitative metrics in Table 1.

4. Discussion

Our study proposes the FAD-FWI framework, an innovative approach to FWI that leverages U-Net reparameterization within an RNN-based paradigm. This approach demonstrates potential in handling challenging scenarios where conventional FWI struggles, such as noisy seismic data with missing low-frequency components and imprecise initial models. While the results affirm the robustness and flexibility of FAD-FWI, the method also presents some limitations and potential areas for enhancement. The primary bottleneck of the proposed FAD-FWI framework lies in the memory requirements associated with the RNN-based FWI. Using reverse-mode AD to compute gradients requires storing intermediate variables at each step, which significantly increases memory demands.[9,25,49] This constraint can be addressed by employing efficient boundary-saving techniques and checkpointing, which reduce memory requirements by selectively saving intermediate steps at the cost of increased computational overhead.[49] Balancing this trade-off between memory and computational demand is crucial for scaling FAD-FWI to larger, more complex models.

Furthermore, our FAD-FWI framework is general and

flexible, providing a foundation for integrating DNN-based parameterization and reformulation within FWI workflows. This versatility suggests promising applications beyond single-physics inversion. The framework can be extended to multi-physics coupled inversion and multi-data joint inversion, allowing for the incorporation of complementary data types (*e.g.*, electromagnetic, gravitational) to improve the resolution and accuracy of subsurface models.[9,50,51] Such extensions could enhance imaging and characterization in diverse geophysical applications, from reservoir monitoring to mineral exploration. In summary, the proposed FAD-FWI framework addresses some key challenges in FWI and shows potential for broad applicability. Future work will focus on optimizing memory efficiency and extending the FAD-FWI framework to multi-physics and joint inversion scenarios, further advancing seismic inversion and subsurface imaging capabilities in geophysics.

5. Conclusion

This study introduces a novel FAD-FWI framework that couples U-Net reparameterization within an RNN-based paradigm. Through a series of experiments, we demonstrated the superiority of our proposed FAD-FWI over conventional DW-FWI approach without DNN reparameterization, highlighting its robustness in scenarios with inaccurate initial models and in the presence of uncertainties in seismic observations, such as noise and missing frequency components. Recovering a velocity model from noisy seismic observations that lack low-frequency components and begin with a rough initial model is typically very challenging for conventional FWI methods. However, our proposed FAD-FWI achieves impressive performance in this demanding scenario. Our findings underscore the potential of deep learning techniques to significantly improve seismic inversion processes, thereby advancing subsurface imaging capabilities and contributing to more accurate geophysical explorations.

Acknowledgments

None.

Funding

This work was financially supported by the National Natural Science Foundation of China Program (42327803, 42304121, 42574154, U2344218), the Open Fund of National Engineering Research Center of Oil and Gas Exploration Computer Software, and the Natural Science Foundation of Wuhan (2025040601020137).

Conflict of interest

The authors declare that they have no competing interests.

Author contributions

Conceptualization: Yufeng Wang
Formal analysis: Jingyi Zhao, Ying Yang
Investigation: Pengyuan Sun, Jun Zheng, Ying Yang
Methodology: Pengyuan Sun, Yufeng Wang
Visualization: Jun Zheng, Ying Yang
Writing–original draft: Pengyuan Sun, Jingyi Zhao
Writing–review & editing: Jingyi Zhao, Yufeng Wang

Availability of data

Data are available from the corresponding author upon reasonable request.

References

1. Tarantola A. Inversion of seismic reflection data in the acoustic approximation. *Geophysics*. 1984;49(8):1259-1266.

   doi: 10.1190/1.1441754

2. Virieux J, Operto S. An overview of full-waveform inversion in exploration geophysics. *Geophysics*. 2009;74(6): WCC1-WCC26.

   doi: 10.1190/1.3238367

3. Zhang X, Lomas A, Zhou M, Zheng Y, Curtis A. 3-D Bayesian variational full waveform inversion. *Geophys J Int*. 2023;234(1):546-561.

   doi: 10.1093/gji/ggad057

4. Plessix RE. A review of the adjoint-state method for computing the gradient of a functional with geophysical applications. *Geophys J Int*. 2006;167(2):495-503.

   doi: 10.1111/j.1365-246X.2006.02978.x

5. Wang T, Cheng J, Geng J. Reflection full waveform inversion with second-order optimization using the adjoint-state method. *J Geophys Res Solid Earth*. 2021;126(8).

   doi: 10.1029/2021jb022135

6. Li YE, Demanet L. Full-waveform inversion with extrapolated low-frequency data. *Geophysics*. 2016;81(6):R339-R348.

   doi: 10.1190/geo2016-0038.1

7. Métivier L, Allain A, Brossier R, Mérigot Q, Oudet E, Virieux J. Optimal transport for mitigating cycle skipping in full-waveform inversion: A graph-space transform approach. *Geophysics*. 2018;83(5):R515-R540.

   doi: 10.1190/geo2017-0807.1

8. Teodor D, Comina C, Khosro Anjom F, Brossier R, Socco LV, Virieux J. Challenges in shallow target reconstruction by

3D elastic full-waveform inversion - which initial model? *Geophysics*. 2021;86(4):R433-R446.

doi: 10.1190/geo2019-0523.1

9. Li D, Xu K, Harris JM, Darve E. Coupled time-lapse full-waveform inversion for subsurface flow problems using intrusive automatic differentiation. *Water Resour Res*. 2020;56(8):e2019WR027032.

doi: 10.1029/2019wr027032

10. Zhu W, Xu K, Darve E, Beroza GC. A general approach to seismic inversion with automatic differentiation. *Comput Geosci*. 2021;151:104751.

doi: 10.1016/j.cageo.2021.104751

11. Adler A, Araya-Polo M, Poggio T. Deep learning for seismic inverse problems: Toward the acceleration of geophysical analysis workflows. *IEEE Signal Process Mag*. 2021;38(2): 89-119.

doi: 10.1109/msp.2020.3037429

12. Yu S, Ma J. Deep learning for geophysics: Current and future trends. *Rev Geophys*. 2021;59(3):e2021RG000742.

doi: 10.1029/2021rg000742

13. Yang F, Ma J. Deep-learning inversion: A next generation seismic velocity-model building method. *Geophysics*. 2019;84(4):R583-R599.

doi: 10.1190/geo2018-0249.1

14. Deng C, Feng S, Wang H, *et al*. OpenFWI: Large-scale multi-structural benchmark datasets for full waveform inversion. *Adv Neural Inf Process Syst*. 2022;35:6007-6020.

15. Lewis W, Vigh D. Deep Learning Prior Models from Seismic Images for Full-Waveform Inversion. In: *SEG International Exposition and Annual Meeting*. SEG; 2017.

16. Sun H, Demanet L. Extrapolated full-waveform inversion with deep learning. *Geophysics*. 2020;85(3):R275-R288.

doi: 10.1190/geo2019-0195.1

17. Zhang W, Gao J, Gao Z, Chen H. Adjoint-driven deep-learning seismic full-waveform inversion. *IEEE Trans Geosci Remote Sens*. 2020;59(10):8913-8932.

doi: 10.1109/tgrs.2020.3044065

18. Zhang ZD, Alkhalifah T. High-resolution reservoir characterization using deep learning-aided elastic full-waveform inversion: The North Sea field data example. *Geophysics*. 2020;85(4):WA137-WA146.

doi: 10.1190/geo2019-0340.1

19. Li Y, Alkhalifah T, Zhang Z. Deep-learning assisted regularized elastic full waveform inversion using the velocity distribution information from wells. *Geophys J Int*. 2021;226(2):1322-1335.

doi: 10.1093/gji/ggab162

20. Wang F, Huang X, Alkhalifah TA. A prior regularized full waveform inversion using generative diffusion models. *IEEE Trans Geosci Remote Sens*. 2023;61:1-11.

doi: 10.1109/tgrs.2023.3337014

21. Feng S, Lin Y, Wohlberg B. Multiscale data-driven seismic full-waveform inversion with field data study. *IEEE Trans Geosci Remote Sens*. 2021;60:1-14.

doi: 10.1109/tgrs.2021.3114101

22. Rasht-Behesht M, Huber C, Shukla K, Karniadakis GE. Physics-informed neural networks (PINNs) for wave propagation and full waveform inversions. *J Geophys Res Solid Earth*. 2022;127(5):e25.

doi: 10.1029/2021jb023120

23. Richardson A. *Seismic Full-Waveform Inversion Using deep Learning Tools and Techniques*. [arXiv Preprint]; 2018.

doi: 10.48550/arXiv.1801.07232

24. Yang Y, Gao AF, Azizzadenesheli K, Clayton RW, Ross ZE. Rapid seismic waveform modeling and inversion with neural operators. *IEEE Trans Geosci Remote Sens*. 2023;61:1-12.

doi: 10.1109/tgrs.2023.3264210

25. Sun J, Niu Z, Innanen KA, Li J, Trad DO. A theory-guided deep-learning formulation and optimization of seismic waveform inversion. *Geophysics*. 2020;85(2):R87-R99.

doi: 10.1190/geo2019-0138.1

26. Song C, Wang Y, Richardson A, Liu C. Weighted envelope correlation-based waveform inversion using automatic differentiation. In: *IEEE Transactions on Geoscience and Remote Sensing*. Vol. 61. New York: IEEE; 2023.

doi: 10.1109/tgrs.2023.3300127

27. Fang J, Zhou H, Elita Li Y, Shi Y, Li X, Wang E. Deep-learning optimization using the gradient of a custom objective function: A full-waveform inversion example study on the convolutional objective function. *Geophysics*. 2024;89(5):R479-R492.

doi: 10.1190/geo2023-0538.1

28. Zhang Y, Zhu X, Gao J. Seismic inversion based on acoustic wave equations using physics-informed neural network. *IEEE Trans Geosci Remote Sens*. 2023;61:1-11.

doi: 10.1109/tgrs.2023.3236973

29. Schuster GT, Chen Y, Feng S. Review of physics-informed machine-learning inversion of geophysical data. *Geophysics*. 2024;89(6):1-91.

doi: 10.1190/geo2023-0615.1

30. Li Z, Kovachki N, Azizzadenesheli K, *et al*. *Fourier Neural Operator for Parametric Partial Differential Equations*. [arXiv Preprint]; 2020.

doi: 10.48550/arxiv.2010.08895

31. Lu L, Jin P, Pang G, Zhang Z, Karniadakis GE. Learning nonlinear operators via DeepONet based on the universal approximation theorem of operators. *Nat Mach Intell*. 2021;3(3):218-229.

32. Guo Z, Chai L, Huang S, Li Y. *Inversion-DeepONet: A Novel DeepONet-Based Network with Encoder-Decoder for Full Waveform Inversion*. [arXiv Preprint]; 2024.

    doi: 10.48550/arXiv.2408.08005

33. Ulyanov D, Vedaldi A, Lempitsky V. Deep Image Prior. In: *Proceedings of the IEEE Conference on Computer Vision and Pattern Recognition*; 2018. p. 9446-9454.

34. Dittmer S, Kluth T, Maass P, Baguer DO. Regularization by architecture: A deep prior approach for inverse problems. *J Math Imaging Vision*. 2020;62:456-470.

35. Xie Y, Chen W, Ge H, Ng MK. Deep image prior and weighted anisotropic-isotropic total variation regularization for solving linear inverse problems. *Appl Math Comput*. 2024;482:128952.

    doi: 10.1016/j.amc.2024.128952

36. Wu Y, McMechan GA. Parametric convolutional neural network-domain full-waveform inversion. *Geophysics*. 2019;84(6):R881-R896.

    doi: 10.1190/geo2018-0224.1

37. He Q, Wang Y. Reparameterized full-waveform inversion using deep neural networks. *Geophysics*. 2021;86(1): V1-V13.

    doi: 10.1190/geo2019-0382.1

38. Zhu W, Xu K, Darve E, Biondi B, Beroza GC. Integrating deep neural networks with full-waveform inversion: Reparametrization, regularization, and uncertainty quantification. *Geophysics*. 2022;87(1):R93-R109.

    doi: 10.1190/geo2020-0933.1

39. Dhara A, Sen MK. Elastic full-waveform inversion using a physics-guided deep convolutional encoder-decoder. In: *IEEE Transactions on Geoscience and Remote Sensing*. New York: IEEE; 2023.

    doi: 10.1109/tgrs.2023.3294427

40. Sun J, Innanen K, Zhang T, Trad D. Implicit seismic full waveform inversion with deep neural representation. *J Geophys Res Solid Earth*. 2023;128(3):e2022JB025964.

    doi: 10.1029/2022jb025964

41. Herrmann L, Bürchner T, Dietrich F, Kollmannsberger S. On the use of neural networks for full waveform inversion. *Comput Methods Appl Mech Eng*. 2023;415:116278.

    doi: 10.1016/j.cma.2023.116278

42. Arridge S, Maass P, Öktem O, Schönlieb CB. Solving inverse problems using data-driven models. *Acta Numerica*. 2019;28:1-174.

    doi: 10.1017/s0962492919000059

43. Sun P, Yang F, Liang H, Ma J. Full-waveform inversion using a learned regularization. In: *IEEE Transactions on Geoscience and Remote Sensing*. New York: IEEE; 2023.

    doi: 10.1109/tgrs.2023.3322964

44. Lord GJ, Powell CE, Shardlow T. *An Introduction to Computational Stochastic PDEs*. Vol. 50. Cambridge: Cambridge University Press; 2014.

45. Benitez JAL, Furuya T, Faucher F, Tricoche X, Hoop M. *Fine-Tuning Neural-Operator Architectures for Training and Generalization*. [arXiv Preprint]; 2023.

46. Ronneberger O, Fischer P, Brox T. *U-net: Convolutional Networks for Biomedical Image Segmentation, in Medical Image Computing and Computer-Assisted Intervention-MICCAI 2015: 18th International Conference, Munich, Germany, 2015, Proceedings, Part III 18*. Berlin: Springer; 2015. p. 234-241.

47. Siddique N, Paheding S, Elkin CP, Devabhaktuni V. U-net and its variants for medical image segmentation: A review of theory and applications. *IEEE Access*. 2021;9:82031-82057.

48. Baydin AG, Pearlmutter BA, Radul AA, Siskind JM. Automatic differentiation in machine learning: A survey. *J Mach Learn Res*. 2018;18(153):1-43.

49. Wang S, Jiang Y, Song P, Tan J, Liu Z, He B. Memory optimization in RNN-based full waveform inversion using boundary saving wavefield reconstruction. *IEEE Trans Geosci Remote Sens*. 2023;61:1-12.

    doi: 10.1109/tgrs.2023.3317529

50. Yin Z, Orozco R, Louboutin M, Herrmann FJ. Solving multiphysics-based inverse problems with learned surrogates and constraints. *Adv Model Simul Eng Sci*. 2023;10(1):14.

51. Liu M, Vashisth D, Grana D, Mukerji T. Joint inversion of geophysical data for geologic carbon sequestration monitoring: A differentiable physics-informed neural network model. *J Geophys Res Solid Earth*. 2023;128(3):e2022JB025372.

    doi: 10.1029/2022jb025372